

See discussions, stats, and author profiles for this publication at: <https://www.researchgate.net/publication/257193170>

# Functionalized silica–chitosan hybrid membrane for dehydration of ethanol/water azeotrope: Effect of cross-linking on structure and performance

ARTICLE *in* JOURNAL OF MEMBRANE SCIENCE · OCTOBER 2013

Impact Factor: 5.06 · DOI: 10.1016/j.memsci.2013.04.065

---

CITATIONS

11

---

READS

201

## 2 AUTHORS:



Ravi Prakash Pandey

Central Salt and Marine Chemicals Researc...

12 PUBLICATIONS 46 CITATIONS

[SEE PROFILE](#)

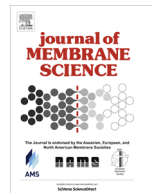


Vinod K. Shahi

Central Salt and Marine Chemicals Researc...

130 PUBLICATIONS 3,330 CITATIONS

[SEE PROFILE](#)



# Functionalized silica–chitosan hybrid membrane for dehydration of ethanol/water azeotrope: Effect of cross-linking on structure and performance



Ravi P. Pandey <sup>a,b</sup>, Vinod K. Shahi <sup>a,b,\*</sup>

<sup>a</sup> Academy of Scientific and Innovative Research, India

<sup>b</sup> Electro-Membrane Processes Division, CSIR-Central Salt & Marine Chemicals Research Institute, G.B. Marg, Bhavnagar-364002, Gujarat, India

## ARTICLE INFO

### Article history:

Received 21 February 2013

Received in revised form

11 April 2013

Accepted 29 April 2013

Available online 18 May 2013

### Keywords:

N-o-sulphonic acid benzyl chitosan

Polysiloxane

Tunable cross-linking

Dehydration of ethanol

Pervaporation

## ABSTRACT

Sodium 2-formylbenzenesulfonatepolysiloxane (SBAPTS) was synthesized, while chitosan was modified to *N*-o-sulphonic acid benzyl chitosan (NSBC). NSBC-SBAPTS hybrid membranes were prepared for pervaporation (PV) dehydration of water–ethanol mixture. Grafting of  $-\text{SO}_3\text{H}$  groups was achieved on both segments (organic and inorganic) of hybrid membranes. Membrane composition and cross-linking density were systematically optimized to explore the effect of membrane structure on its PV performance. Most suitable hybrid membrane (CPS-a) showed 0.59 kg/l<sup>2</sup> h permeation flux and 5282 selectivity for dehydration of ethanol (90 wt%) at 30 °C.

© 2013 Elsevier B.V. All rights reserved.

## 1. Introduction

Chitosan, a promising membrane material [1,2], has been widely studied for biomedical applications [3], drug delivery systems [4], sensors [5], solid polymer electrolytes [6], membranes for separations etc. [7]. The presence of hydroxyl and amino groups in glucosamine unit provides the cross-linking sites [8–12]. Cross-linked chitosan based PV membranes showed good stability and were anticipated to be suitable for the separation of alcohol/water azeotropic mixture [13–15]. However, excessive swelling and low water-permselectivity of chitosan based PV membrane are serious problems [16].

Diversified efforts, such as blending of chitosan with another polymer [17], doping of inorganic filler in the chitosan matrix [18], chitosan based organic–inorganic hybrid [19], or modification of chitosan, were reported [20]. Chitosan-hetopoly acid ( $\text{H}_{14}[\text{NaP}_5\text{W}_{30}\text{O}_{110}]$ ) nanoparticle impregnated membrane with high water-permselectivity was also reported [21]. Blending or doping of inorganic filler in chitosan membrane leads to leaching-out problems. For good interaction between chitosan and inorganic

part, chitosan was functionalized either by introducing quaternary ammonium groups [22] or carboxylic acid groups [23]. Although, functionalized silica nanoparticles were used to develop chitosan based organic–inorganic hybrid membranes [18], sulphonic acid functionalized chitosan has been not reported.

Silica nanoparticle derived membrane showed high permeability and permselectivity for small molecules (such as water (kinetic diameter 2.6 Å)), while relatively low permeability for larger molecules (> 3 Å) (such as ethanol) [24]. Sulphonic acid functionalized silica nanoparticles served as reactive sites for chitosan cross-linking resulting in homogeneous dispersion and swollen stability responsible for high water permselectivity [18]. The PV performances of sulphonic acid functionalized chitosan and silica precursor based organic–inorganic hybrid membranes are still unexplored. Attractive features of these membranes, such as arrangement of silica, interfacial junction between functionalized organic and inorganic segments and membrane hydrophilic nature, will be responsible for preferential sorption and diffusion of water across the membrane.

Herein, first time we are reporting NSBC–SBAPTS hybrid membrane with improved permeability and selectivity for dehydration of ethanol. Poly(vinyl alcohol) (PVA) was used as a plasticizer because of its alcohol impervious and stable nature. Acetalization of oxidative sensitive primary alcohol groups by formal reaction (cross-linking) leads to more stable ether-type linkages [25].

\* Corresponding author at: Electro-Membrane Processes Division, CSIR-Central Salt & Marine Chemicals Research Institute, G.B. Marg, Bhavnagar-364002, Gujarat, India. Tel.: +91 278 2569445; fax: +91 278 2567562/2566970.

E-mail addresses: [vksahai@csmcri.org](mailto:vksahai@csmcri.org), [vinodshahi1@yahoo.com](mailto:vinodshahi1@yahoo.com) (V.K. Shahi).

## 2. Experimental

### 2.1. Materials

Deacetylated chitosan (100% deacetylated), 2-sulphonic acid benzaldehyde, and (3-Aminopropyl) triethoxysilane (APTES) were purchased from Sigma Aldrich chemicals and used without any purification. Poly(vinyl alcohol) (PVA; MW, 125 000; degree of polymerization, 1700; degree of hydrolysis, 88%), methanol, acetic acid, sodium borohydride, formaldehyde, hydrogen peroxide, etc., of AR grade were obtained from SD fine chemicals, India, and used with proper purification. In all experiments, milli-Q water was used.

### 2.2. Surface functionalization of silica nanoparticles

Preparation procedure for SBAPTS has been included in Scheme 1 [26]. 3-aminopropyltrimethoxysilane (APTES) (6 mL) was mixed with THF/isopropanol (2/1 mixture) (80 mL) in a round-bottom flask. Further, THF solution (30 mL) containing sodium 2-formylbenzenesulfonate (5.6 g) was added drop-wise under stirring for 6 h at 60 °C. Then, 0.1 M HCl (5 mL) was added for the polymerization. Further sodium borohydride (5% w/v) was added under stirred condition (4 h) to reduce the imine linkage. After complete evolution of hydrogen, suspended particles were filtered. Filtrate was added to 20-fold acetone to precipitate the polymer. Obtained precipitate was washed several times with acetone and dried under vacuum. The prepared polymer was named as (SBAPTS-X), where X stands for the degree of substitution of the polysiloxane by sodium 2-formylbenzenesulfonate.

### 2.3. Synthesis of N-o-sulphonic acid benzyl chitosan

N-o-sulphonic acid benzyl chitosan (NSBC) was synthesized by Schiff base formation reaction (Scheme S1, (Supporting information)) [6]. In a typical synthetic procedure, chitosan (high viscosity grade) was dissolved in aq. acetic acid solution (0.7 wt %) at pH 3. After complete dissolution of chitosan, sodium 2-formylbenzenesulfonate (3 equiv.) was added. Obtained mixture was refluxed at 60 °C under 4–7 h constant stirring. After completion of reaction, pH was slowly increased up to 4–5. Further aqueous solution of sodium borohydride (5% w/v) was added drop-wise to complete reduction of imine linkage (assured by disappearance of gases evolution). Reduced product was precipitated with methanol and washed by ethyl alcohol and deionized water to remove the last trace of un-reacted sodium borohydride. The prepared polymer was named as (NSBC-X), where X stands for the degree of substitution of the chitosan by sodium 2-formylbenzenesulfonate.

### 2.4. Membrane preparation

NSBC-SBAPTS hybrid membranes were prepared by sol-gel in two steps (Fig. S1 (Supporting information)). NSBC (2.0 g) was dissolved in hot deionized water (50 mL) in presence of HCl (0.1 M) under constant stirring, to obtain a highly viscous solution. PVA (2.0 g in 20 mL) solution was prepared in deionized water at 70 °C separately, while polysiloxane (2.0 mL) solution in deionized water (20 mL) under constant stirring was also prepared separately. All these solutions were mixed under stirred conditions at room temperature and kept overnight to obtain a clear solution. Obtained solution was transformed into a thin film and dried at ambient temperature for 24 h followed by keeping it in vacuum oven at 60 °C for another 24 h. These membranes were cross-linked under different conditions (varied time, concentration of formal solution ( $\text{HCHO} + \text{H}_2\text{SO}_4$ ) and temperature). Resultant

membranes were designated as CPS-X, where X is the cross-linking condition. Eight membranes were prepared under different cross-linking conditions for further characterization.

### 2.5. Instrumental characterization of the membranes

FTIR spectra of dried membrane samples were recorded by Spectrum GX series 49387 spectrometer in the range of 4000–450  $\text{cm}^{-1}$ . The IR spectrum for synthesized intermediate was obtained by the KBr pellet method. Wide angle X-ray diffractograms of the hybrid membranes were recorded using Philips Xpert X-ray diffractometer with Cu K $\alpha$  (1.54056) radiation.  $^1\text{H}$  and  $^{13}\text{C}$  were used to characterize the synthesized material by NMR spectrometer (Bruker500 MHz) in a  $\text{D}_2\text{O}$  and  $d_6\text{-DMSO}$  solvent.

Thermal stability of the membranes was investigated by thermogravimetric analyzer (Mettler Toledo TGA/SDTA851 with Star software) under a nitrogen atmosphere with a heating rate of 10 °C/min from 30 to 450 °C. Differential scanning calorimetry (DSC) measurements were carried out between 30 and 450 °C with 5 °C/min heating rate. The dynamic mechanical stability of hybrid membranes was evaluated by using a Mettler Toledo dynamic mechanical analyzer 861 instruments with Star<sup>c</sup> software under nitrogen with 10 °C/min heating rate from 30 to 320 °C.

The surface morphology of dried membranes was studied by a JEOL 1200EX transmission electron microscope (TEM) with tungsten, and electron source operated at an accelerating voltage of up to 120 kV. Atomic force microscopy (AFM) images of dried membranes were recorded using NTEGRA AURA (NTMDT). Semi-contact mode SPM NSG 01 tip (radius of curvature: 10 nm, and frequency for cantilever: 300 kHz) was used to determine the surface roughness. Tip was located with cantilever, and oscillates with natural frequency, while sample topography was obtained from the subsequent changes in the oscillation amplitude. Differences in viscoelastic properties were detected by the change in the oscillation phase. For scanning electron microscopy (SEM), gold sputter coating was carried out on desired membrane samples at pressure ranging in between 1 and 0.1 Pa. Sample was loaded in the machine, which was operated at  $10^{-2}$ – $10^{-3}$  Pa with EHT 15.00 kv with 300 V collector bias using Leo microscope. SEMs were recorded.

### 2.6. Membrane swelling

Dry membrane samples of known weight were equilibrated in pure solvent for 72 h. The swollen membrane was wiped with tissue paper to remove adherent solvent and weighed for the estimation of swelling ratio using the equation [23]:

$$S(\%) = \frac{W_s - W_d}{W_d} \times 100 \quad (1)$$

where,  $W_d$  denotes the weight of the dry membrane and  $W_s$  denotes the weight of solvent swollen membrane.

### 2.7. Pervaporation experiments

Pervaporation apparatus has been schematically described in Fig. S2 (Supporting information). The cell assembled for two half cells of column couplers were made of steel and fastened with bolts. The capacity of each cell was about 50 mL and the effective area of the membrane was 12.56  $\text{cm}^2$ . The membrane was supported on a finely porous copper plate with 100  $\mu\text{m}$  porosity. Vacuum in the down-stream side was measured with a vacuum gauge. The membrane was equilibrated for 2 h in the cell before experiments and the permeated samples were collected after 2 h. In the permeate side, vapours were completely condensed in a trap placed in a liq. nitrogen cylinder. Permeate and feed

compositions were analyzed by refractive index. Pervaporation experiments were carried out at different temperatures (30 and 50 °C) using freshly prepared feed solution, in triplicate. Permeation rate or flux ( $J$ ) was calculated from the weight of permeate collected after pervaporation run from the following equation:

$$J = \frac{Q}{At} \quad (2)$$

where  $Q$  is the quantity (kilograms) of permeate collected after time ( $t$ ) and  $A$  is the effective membrane area. General procedures for the estimation of permeability and selectivity are included in Section S1 (Supporting information) [23].

### 3. Results and discussion

#### 3.1. Structure of monomer precursor and hybrid membrane

Polysiloxane (SBAPTS) was synthesized by the Schiff base reaction using sodium 2-formylbenzenesulfonate and APTEOS.  $^1\text{H}$  NMR spectra of SBAPTS showed shift at 0.607 ppm for Si-CH<sub>2</sub>-protons. Modification of polysiloxane was confirmed by peaks at 7.22, 7.48, 7.73 and 8.13 ppm due to phenyl ring and other protons shifts (Fig. 1). In  $^{13}\text{C}$  NMR spectra, peaks at 127.50–144.70 ppm, and 67.62 ppm were assigned to phenyl ring and Ph-CH<sub>2</sub> groups, respectively. Carbons shifts for –OCH<sub>2</sub>CH<sub>3</sub> were observed at 61.29 and 24.36 ppm (Fig. 2). Substitution of 2-formylbenzenesulfonate was confirmed by absorption bands at 1021, 1189, and 1650–2158 cm<sup>-1</sup> due to the presence of sulphonic acid groups (sym. SO<sub>3</sub> Streh.; asym. SO<sub>3</sub> Streh.; –OH stretch.) (Fig. S3, Supporting information) [27]. On the basis of elemental analysis and spectral data structure of polysiloxane (SBAPTS) has been proposed (Scheme 1).

NSBC was synthesized by co-condensation of amine and aldehyde groups via Schiff's base formation. Reduction of Schiff's base with alcoholic sodium borohydride formed the product (Scheme S1, Supporting information). A hydrogen atom from the amino group was substituted by a sodium 2-formylbenzenesulfonate. NSBC new signal at 6.6–7.2 ppm was observed due to the aromatic protons, and a small shift at 7.5 ppm was assigned to the aromatic sulphonic acid group. Other pyranose ring proton and methylene proton (bonded with aromatic ring) are systematically presented

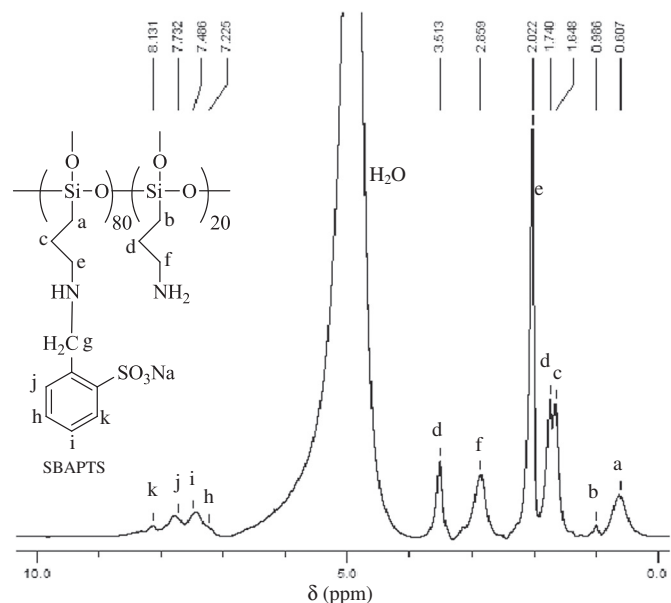


Fig. 1.  $^1\text{H}$  NMR spectrum of synthesized polysiloxane SBAPTS in  $\text{D}_2\text{O}$ .

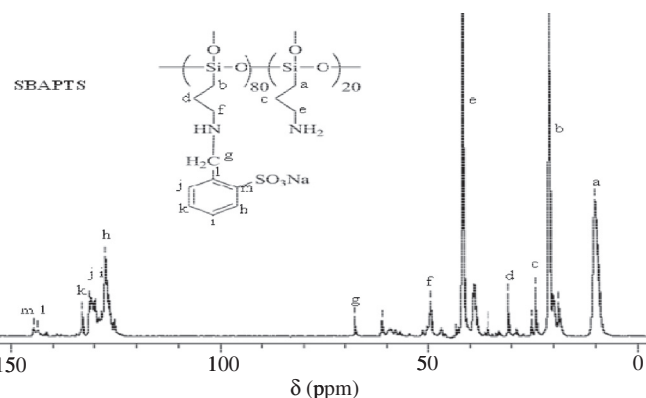
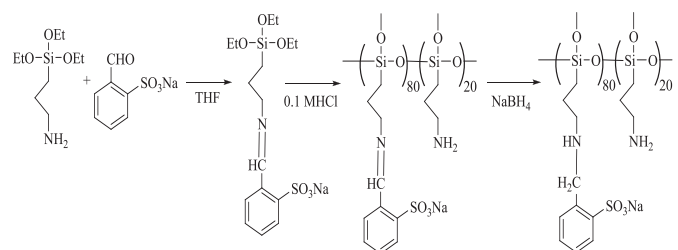


Fig. 2.  $^{13}\text{C}$  NMR spectra of synthesized polysiloxane (SBAPTS) in  $\text{D}_2\text{O}$  and used reference solvent was  $d_6$ -DMSO.



Scheme 1. Reaction involved in the synthesis of polysiloxane (SBAPTS).

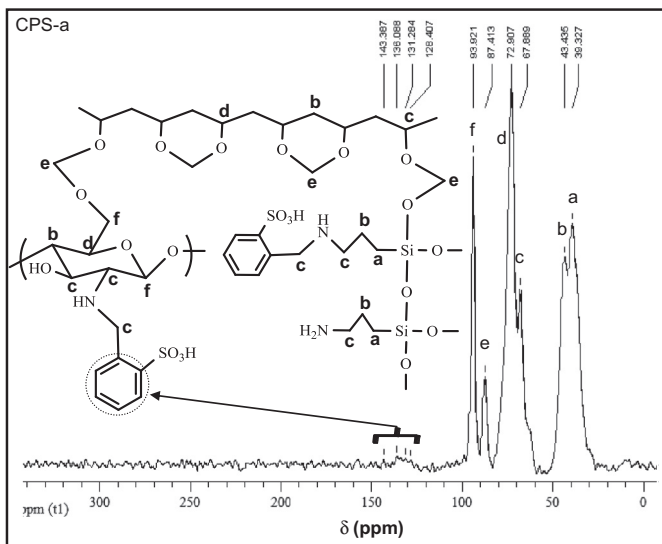
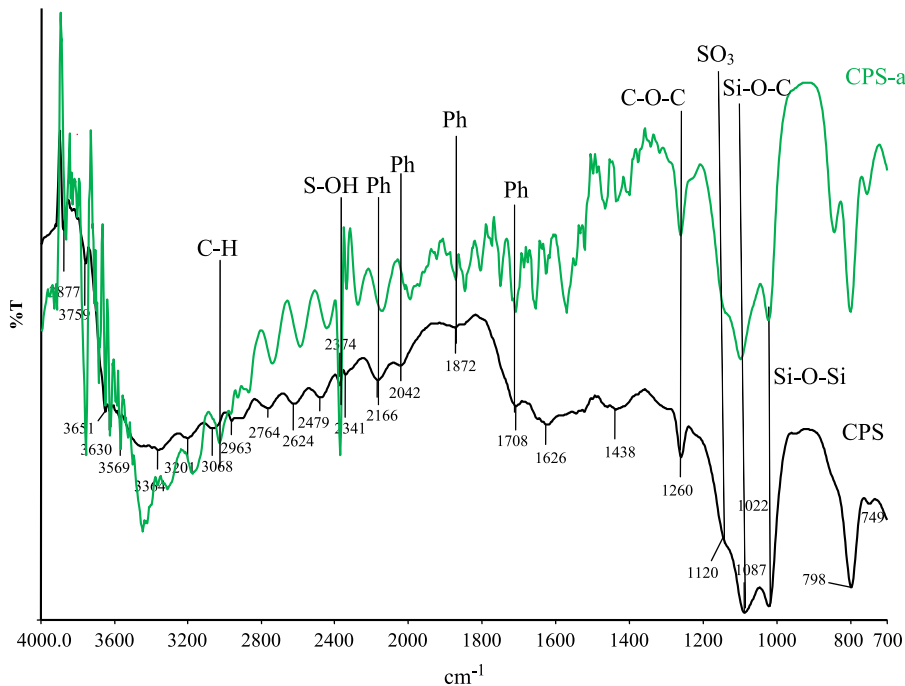


Fig. 3.  $^{13}\text{C}$  NMR spectra of cross-linked membranes.

in Fig. S4 (Supporting information). No reasonable peak was observed in solution state  $^{13}\text{C}$  NMR spectra. Solid state  $^{13}\text{C}$  NMR spectra of NSBC showed two new peaks at 128.46–143.76 and 23.83 ppm due to substitution of –NH<sub>2</sub> protons by 2-formylsulphonic acid. Other carbon shifts are also systematised in Fig. S5 (Supporting information). FTIR spectra showed two new peaks at 1640 and 2040 cm<sup>-1</sup> due to addition of 2-formylsulphonic acid, which also confirmed substitution reaction (Fig. S6, Supporting information). Spectral study confirmed successful substitution of 2-formylbenzenesulfonate, and about 67% conversion of chitosan into NSBC.

Cross-linking of membranes was confirmed by solid state  $^{13}\text{C}$  NMR (Fig. 3 and Fig. S7 (Supporting information)). For uncross-linked membranes, carbon peaks are systematized in Fig. S7 (Supporting information). For cross-linked membranes, additional



**Fig. 4.** FT-ATR spectra of uncross-linked membrane (CPS), and cross-linked membrane (PCS-a).

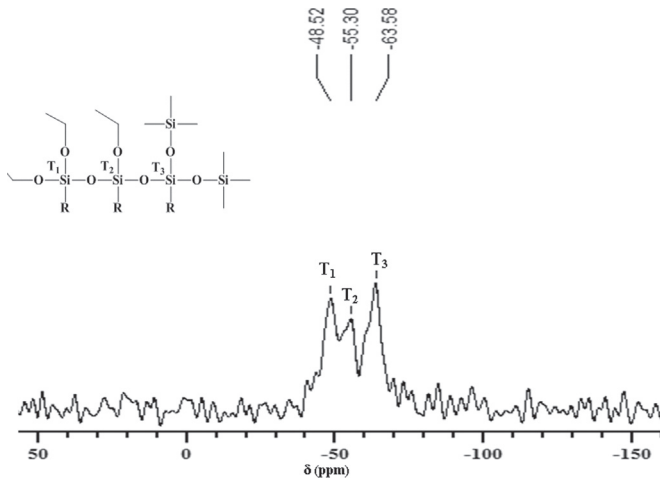


**Fig. 5.** Solid state <sup>29</sup>Si NMR of cross-linked membrane (CPS-a) at 30 °C.

carbon peaks at 39.32, 43.43, 87.41, 93.92 ppm were observed due to cross-linked carbon. FT-ATR spectra for cross-linked hybrid membranes showed strong  $\text{--SO}_3\text{H}$  stretch at  $\nu$ 1120 (sym.  $\text{SO}_3$  stretch),  $\nu$ 1260 (asym.  $\text{SO}_3$  stretch),  $\nu$ 2360–1650 (due to the  $\text{--OH}$  stretching vibration) cm<sup>-1</sup> (Fig. 4). This confirmed successful grafting of sulphonic acid groups [27]. Peaks between 1022 and 1087 cm<sup>-1</sup> were observed due to Si–O–Si and Si–O–C groups [25,28]. An increased absorption intensity of peak at 1087 cm<sup>-1</sup> due to cross-linking was attributed to the increased amount of Si–O–C group. The medium intensity band at 1260 cm<sup>-1</sup> was observed due to C–O–C bonds. The formation of Si–O–C and C–O–C bonds favours better compatibility (between organic and inorganic components) and homogeneity of molecular scale, which is responsible for thermally and mechanically stable membranes. <sup>29</sup>Si-MAS NMR spectra were used to determine the silica nature in the membrane matrix (Fig. 5). The resonances of CPS-a hybrid membrane were assigned to T units aroused from the hydrolysis of SBAPTS. Three peaks (48.52, 55.30, and 63.58 ppm) were assigned to T<sub>1</sub>, T<sub>2</sub> and T<sub>3</sub> types of silica. High intensity of T<sub>3</sub> silica, in comparison with

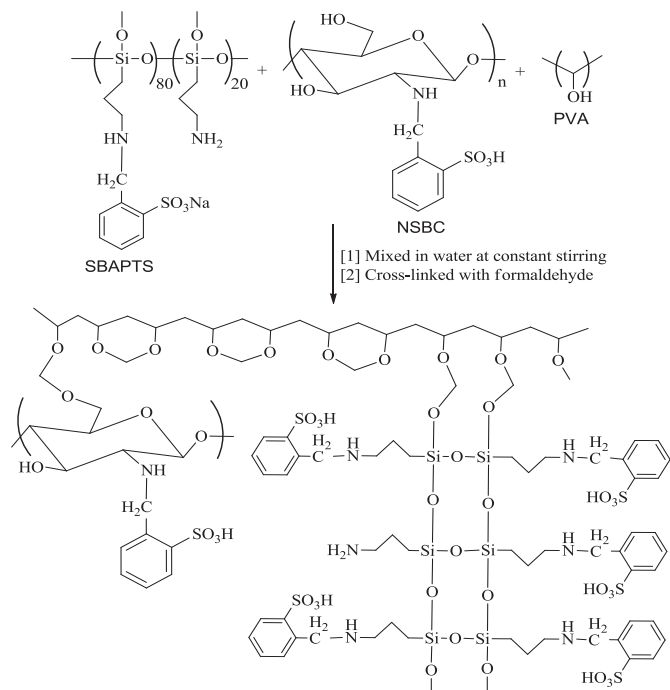


**Fig. 6.** Proposed structure of synthesized membrane (CPS-x).

T<sub>2</sub> and T<sub>1</sub>, indicated sufficient amount of Si–(O–Si)<sub>3</sub> [29]. Based on spectral analysis, schematic membrane structure has been proposed in Fig. 6.

### 3.2. Particle size of silica and structural morphology of membrane

Membranes surface morphology was studied by Optical images, SEM, TEM, and AFM. TEM images for 50 nm fine slice of membrane (CPS-a) was obtained by microtome at –140 °C (Fig. 7). High resolution TEM images showed 0.23–0.33 nm crystal lattice spacing (in close agreement with crystalline silicone) (Fig. 7(d)) [30]. Particle size of silica was estimated to be about 5–14 nm.

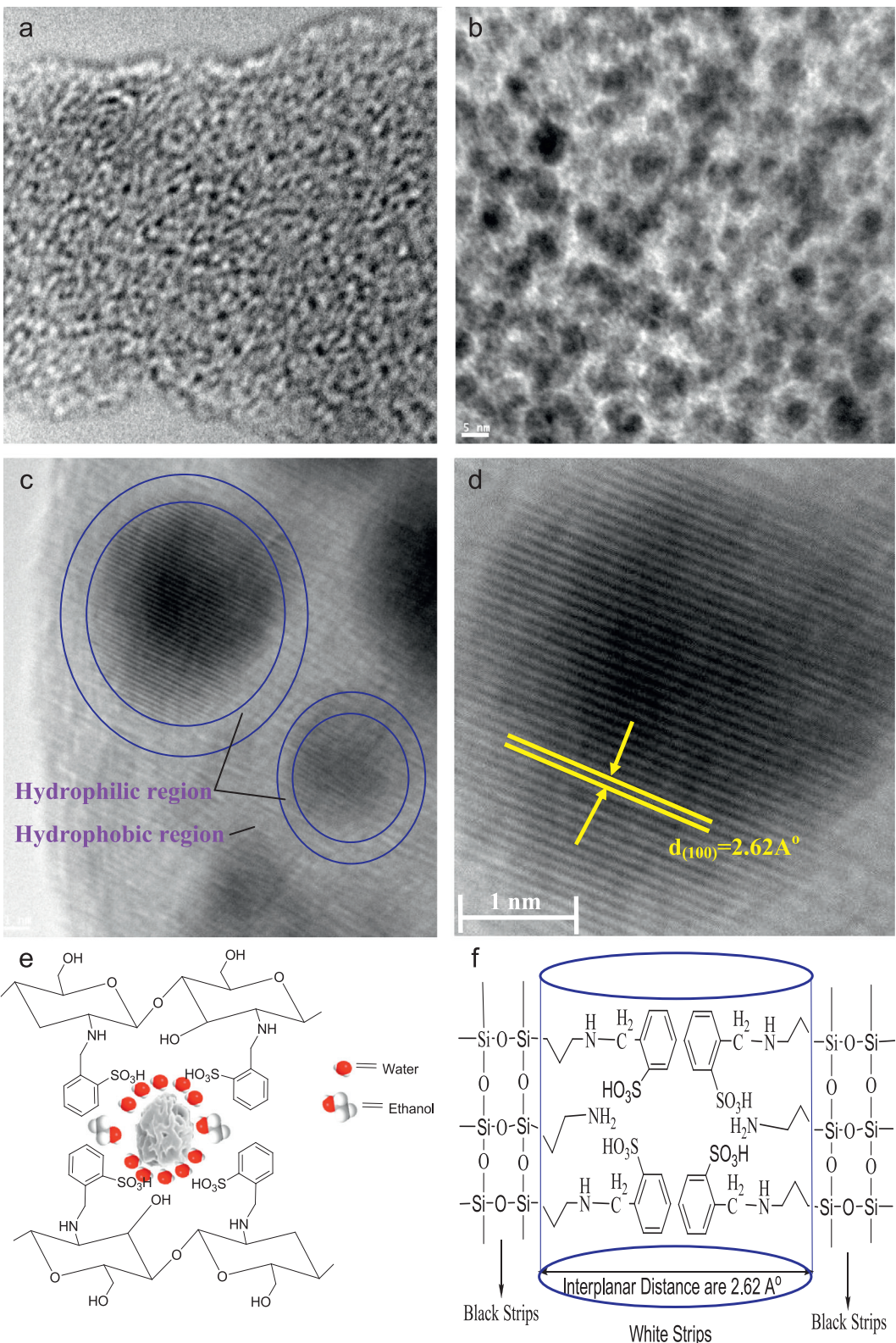


**Fig. 7.** TEM analysis of 50 nm microtome cross-linked membrane; (a, b, c, d) various magnification image; (e) model for hydrophilic channel obtained by chitosan and silica; and (f) model for linearly arranged silica matrix interacted with water molecules.

At high resolution (1 nm bar) clear silica lattice fringes were seen, while in outer side, white patches indicated some vacant portions due to the formation of junction between hydrophilic and hydrophobic segments. For membrane preparation, chitosan was modified as NSBC. Synthesized polysiloxane (SBAPTS) and NSBC both

contained hydrophilic and hydrophobic segments. It is expected that these segments will exhibit the hydrophobic-hydrophobic and hydrophilic-hydrophilic interactions. They may lead the phase separation and are thus responsible for observed black and white strips (Fig. 5(c-f)). This junction plays an important role during

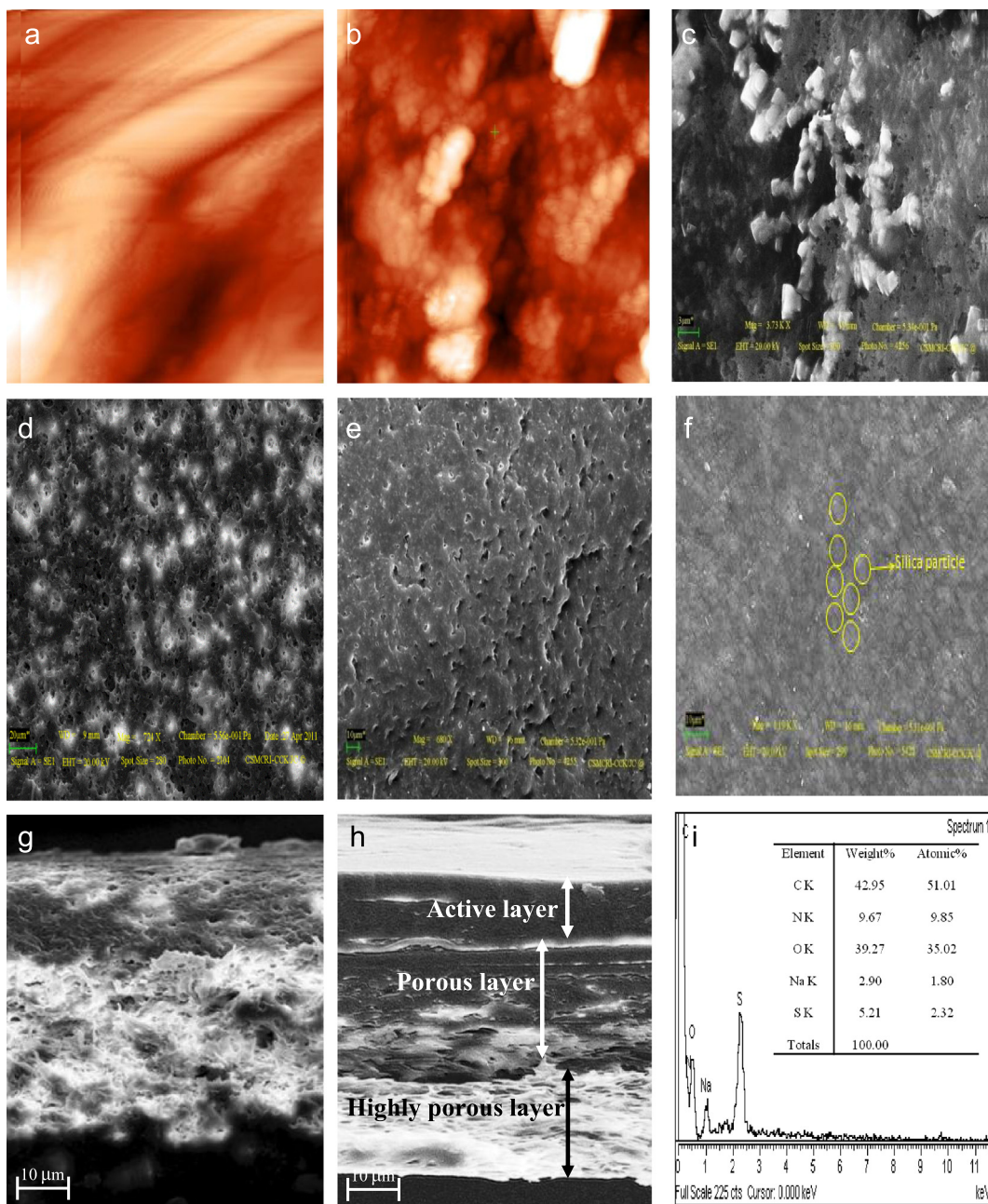


**Fig. 8.** Microscopic analysis of; (a and b) AFM image of CPS and CPS-a (bar scale  $5 \times 5 \mu\text{m}^2$ ; RMS 80 and 130 nm); (c) SEM analyzed surface image of CPS; (d) CPS-f; (e) CPS-e; (f) CPS-a; (g) cross-sectional image of CPS; (h) cross-sectional image of CPS-a; and (i) EDX results of modified chitosan.

separation/pervaporation. Membrane roughness favours high surface area and thus high flux and selectivity for pervaporation membrane. Small pieces of membranes were pasted over the sample grid for AFM scanning (Fig. 8a and b, Fig. S8, Supporting information). Surface roughness was calculated in terms of  $R_q$  (classical amplitude parameter used to assess the surface texture), which measures the average length between peaks and valleys. Surface roughness values for uncross-linked (CPS) and cross-linked (CPS-a) membrane (80 and 130 nm, respectively) conformed increase in membrane surface roughness with cross-linking. Membrane with high surface roughness (surface area) possessed more contacting sites; thus membrane selectivity was affected by cross-linking conditions.

SEM and optical images for CPS, and CPS-a membranes (Fig. 8 and Fig. S9, Supporting information), showed transparent nature of uncross-linked membrane, without any macro-phase separation

with homogeneously distributed silica in membrane matrix. The homogenous distributions of silica particle were also confirmed by the EDX silica mapping (Fig. S9(g), Supporting information), which indicates equivalent distribution of silica particle. After cross-linking, membrane lost its transparency may be due to the formation of covalent bonding (C–O–C groups and Si–O–C) between organic and inorganic segments. Membrane compactness was also increased with cross-linking (Fig. 8c-h); thus free volume within the membrane matrix can be controlled by varying cross-linking conditions.

### 3.3. Thermal, mechanical, and chemical stability

Thermal stability for NSBC, SBAPTS, pristine PVA, uncross-linked, and cross-linked hybrid membranes were analyzed by TGA curves (Fig. S10, Supporting information). SBAPTS showed

one-step weight loss at 270–320 °C, because of de-sulphonation, while NSBC exhibited three-steps weight loss at 30–110, 270–371, and 400–500 °C, which were attributed to the dehydration, de-sulphonation and decomposition of modified chitosan respectively. Pristine PVA membrane also showed two-steps weight losses at 30–150 °C and 270–500 °C due to dehydration and decomposition of modified chitosan respectively. Uncross-linked membrane (CPS) showed three steps weight losses at 30–170 °C, 200–320 °C, and 400–500 °C, which were due to loss in water, functional groups (sulphonic acid, hydroxyl group etc.), and decomposition of pyranose ring of chitosan moiety respectively. In case of cross-linked membrane (CPS-a) weight loss (%) was about 1.35 times higher in comparison with weight loss of uncross-linked membrane (CPS); this confirmed improved thermal resistant nature of the former. The water retention capacity of NSBC, SBAPTS, pristine PVA, uncross-linked and cross-linked membranes (Fig. 9) showed high values for NSBC, while low for SBAPTS. After cross-linking, relatively high weight loss at 200 °C indicated decrease in swelling ratio.

DSC thermograms in the N<sub>2</sub> environment of representative hybrid uncross-linked (CPS) and cross-linked membranes (Fig. S11, Supporting information) showed their *T<sub>g</sub>* values about 95.6, and 59.3 °C, respectively. Incorporation of NSBC in PVA matrix had profound effect on *T<sub>g</sub>* value. The glass transition temperature of pristine PVA was reported to be 78 °C [31,32]. Variations of *T<sub>g</sub>* values may be explained by the plasticizer effect and degree of cross-linking. The first *T<sub>g</sub>* value for uncross-linked membrane was higher than that for cross-linked membrane due to the loss of ordered arrangements of PVA by addition of NSBC, and thus cross-linking density.

The dynamic mechanical analysis (DMA) for different hybrid membranes at 10 N applied force and 1 Hz confirmed the increase in storage modulus with cross-linking density due to the continuous network within organic polymer matrix. Cross-linking density of membrane ( $\rho$ ) was determined by the following equation [6]:

$$\rho = \frac{E'}{3d\phi RT} \quad (3)$$

where,  $d$  is the membrane density,  $\phi$  is the front factor (where  $\phi=1$ ),  $R$  is universal gas constant, and  $T$  is the absolute temperature. The storage modulus ( $E'$ ) of uncross-linked and cross-linked membranes was determined by DMA at 10 Hz frequency and 40 °C (Fig. 10). Detailed studies were carried out to investigate the effect of cross-linking density because of change in experimental

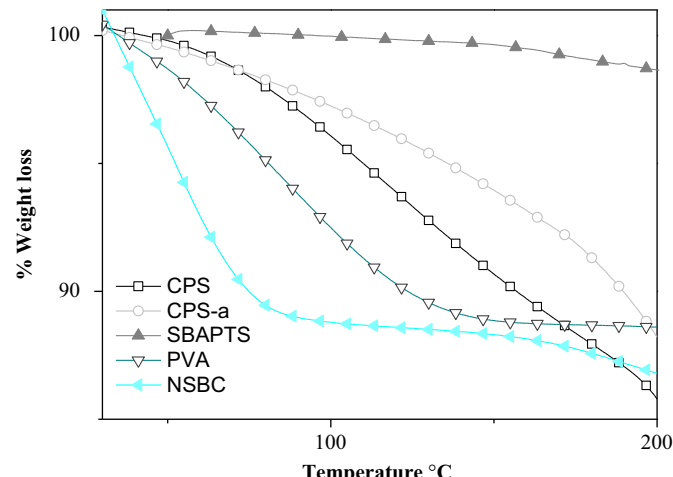


**Fig. 9.** TGA curve showed the rate of water loss for membrane precursors and pervaporation membrane.

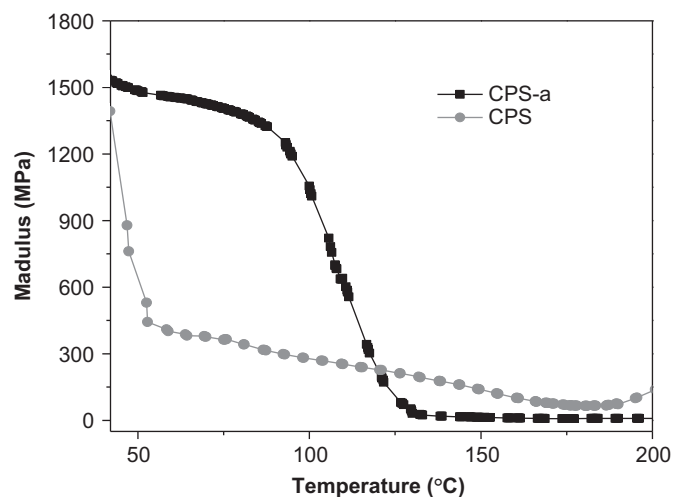


**Fig. 10.** DMA analysis of uncross-linked and cross-linked membrane showed that storage modulus increased with cross-linking condition.

**Table 1**

Membrane preparation conditions with cross-linking density and their contact angles in water and ethanol.

Membrane name	Membrane preparation condition			Cross-linking density (mol g <sup>-1</sup> )	Contact angle (θ)	
	Formaldehyde conc (wt%)	Time (h)	Temperature (°C)		Water	Ethanol
CPS-a	2.5	3	60	0.545	70.32	85.06
CPS-b	2	3	60	0.511	69.32	86.7
CPS-c	1.5	3	60	0.471	68.55	87.14
CPS-d	1	3	60	0.451	68.12	87.64
CPS-e	2.5	2	60	0.496	69.01	86.02
CPS-f	2.5	1	60	0.458	68.32	87.3
CPS-g	2.5	3	50	0.465	68.96	86.23
CPS-h	2.5	3	40	0.466	68.74	86.94

Error limit: Formaldehyde concentration ( $\pm 0.1$  wt%), time ( $\pm 0.05$  h), temperature ( $\pm 1$  °C), cross-linking density ( $\pm 0.001$ ), and contact angle ( $\pm 0.01$ ).

conditions (Table 1). Storage moduli of uncross-linked (CPS) and cross-linked (CPS-a) membranes were considered as moduli at 10 Hz and 40 °C and were found to be about 1.3 and 1.6 GPa, respectively [22].

Cross-linked membrane (CPS-a) showed a peak in tan δ curve (glass transition region) at 134.01 °C, which is comparatively higher than pristine PVA membrane (102 °C) (Fig. S12, Supporting information) [29]. Thus, *T<sub>g</sub>* of the hybrid membrane was shifted towards higher temperature by incorporation of NSBC in the PVA matrix.

### 3.4. Swelling and contact angle

Membrane's behaviour of penetrate (water and ethanol) is an important phenomenon of mass transport, which involves (i) sorption of feed at upstream membrane surface; (ii) diffusion through the membrane and (iii) desorption of permeate as vapour at down-stream membrane surface [33]. Thus, swelling behaviour of hybrid membranes in water and ethanol was studied at different temperatures (Table S1 and Fig. S13 (Supporting information)). Membrane swelling in water was high in comparison with ethanol due to the hydrophilic nature of modified chitosan and silica. Further, membrane swelling increased with time, and after 24 h it was unchanged. Also, hybrid membranes exhibited less swelling ratio in comparison with pristine chitosan membrane,

which may be due to high cross-linking density. Membrane swelling was increased with temperature due to phase change and deformation in polymer structure (**Table 1**).

The membrane hydrophilic nature was studied by contact angle ( $\theta$ ) as a function of cross-linking density (**Table 1**), which was inversely proportional in case of water and directly proportional in case of ethanol. Observed variations in membrane contact angle may be attributed to increased surface smoothness and its hydrophilic nature.

### 3.5. PV results

PV performances of hybrid membranes were studied for dehydration of ethanol (90% (w/w)) at 303 and 323 K. The detailed procedure for the determination of membrane permeability ( $P_w$  and  $P_{EtOH}$ ) is given in **Section S1** (Supporting information). Water and ethanol permeability data ( $P_w$  and  $P_{EtOH}$ ) for different hybrid membranes (varied cross-linking density) are presented in **Fig. 11A** and B. Membrane permeability depends on the protocol of membrane preparation (formaldehyde solution concentration (cross-linking density), and pH of the casting solution) and PV experimental conditions (temperature, membrane thickness feed composition, and pressure etc.). Water and ethanol permeabilities were decreased with cross-linking density due to the increase in dense nature of the membrane. Water permeability decreased, while ethanol permeability increased with temperature, which may be explained on the basis of free volume theory [21]. DSC

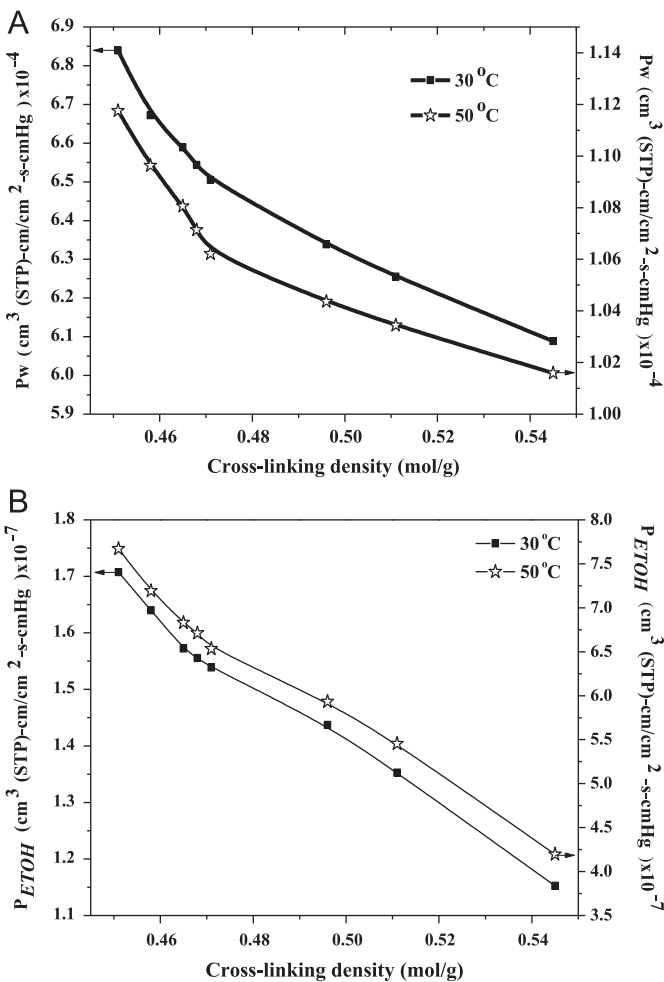


**Fig. 11.** Membrane permeability values through different nanocomposite membrane for; (A) Water ( $P_w$ ); and (B) Ethanol ( $P_{EtOH}$ ), in 90 wt% ethanol at 30 and 50 °C. Measuring error is 1.0%.

analysis also confirmed phase change in the membrane matrix at high temperatures (first endothermic peak at 59 °C indicated deformation in membrane structure), and thus membrane was of temperature sensitive nature. Cross-linked membrane (CPS-a) bears two type of pores, formed by the arrangement of hydrophilic and hydrophobic segments. Relatively small pore size formed by silica permits passage of water molecules, while ethanol molecules (4.46 Å molecular sizes) were blocked, which is responsible for high water selectivity at low temperatures. At high temperatures (50 °C), enhanced free volume in modified chitosan (NSBC) allowed easy permeation of ethanol. Reported membranes showed relatively less contact angle in water (68–70°), in comparison with ethanol (85–87°) (**Table 1**). Hydrogen bond interaction between water and functionalized silica–chitosan hybrid membrane caused preferential sorption and diffusion of water across the membrane. Selectivity data ( $\alpha_{sel}$ ) of CPS-a membrane showed its selective nature (selectivity: 5282 at 30 °C) with high flux (0.59 l m<sup>-2</sup> h) (**Fig. 12**). Furthermore, higher  $\alpha_{sel}$  and flux values for CPS-a membrane suggested its suitability for PV dehydration of ethanol at low temperatures.

Permeabilities of both ( $P_w$  and  $P_{EtOH}$ ) increased quickly with the increase in feed water content (**Fig. 13A**), while selectivity factor decreased steadily (**Fig. 13B**). This may be attributed to the preferential sorption of water molecule because of hydrophilic and charged nature of the membrane surfaces. The charged nature of membrane matrix is playing an important role in the selective sorption of water, which is quite high in comparison with ethanol. Preferential affinity of membranes towards water might have caused membrane swelling and rapid permeation of feed water through the membrane. Consequently, the selectivity parameter values increased rapidly with the increase in NSBC content in the membrane matrix and also with the increase in cross-linking density. Increase in permeability and decrease in selectivity were observed due to hydrophilic membrane nature; therefore more sorption of penetrates on the membrane surface and hydrophilic inorganic region provides favour of diffusion through the membrane. On the other hand selectivity was decreased with increasing amount of water and this may cause more hydrophilic pores to remain open in the polymer matrix and did not differentiate small polarity effects; therefore both ethanol and water molecules easily passed through the membrane matrix. At a high concentration of ethanol hydrophilic pores were closed and water molecules passed through the silica matrix.

PV performances of CPS-a hybrid and other chitosan based membranes for separating water–ethanol mixtures were compared in **Table 2**. Reported functionalized silica–chitosan hybrid membrane shows significant improvement in PV performances over other chitosan based membranes. NCM-5 membrane for

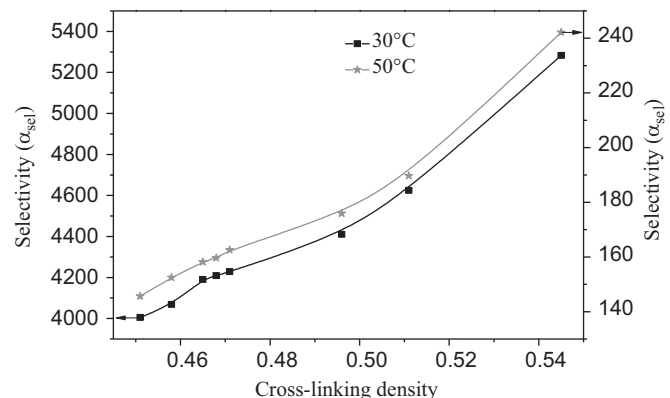


**Fig. 12.** Effect of temperature on selectivity factor for dehydration of ethanol (90 wt %) using different membranes (thickness: 100 µm) at 30 and 50 °C.

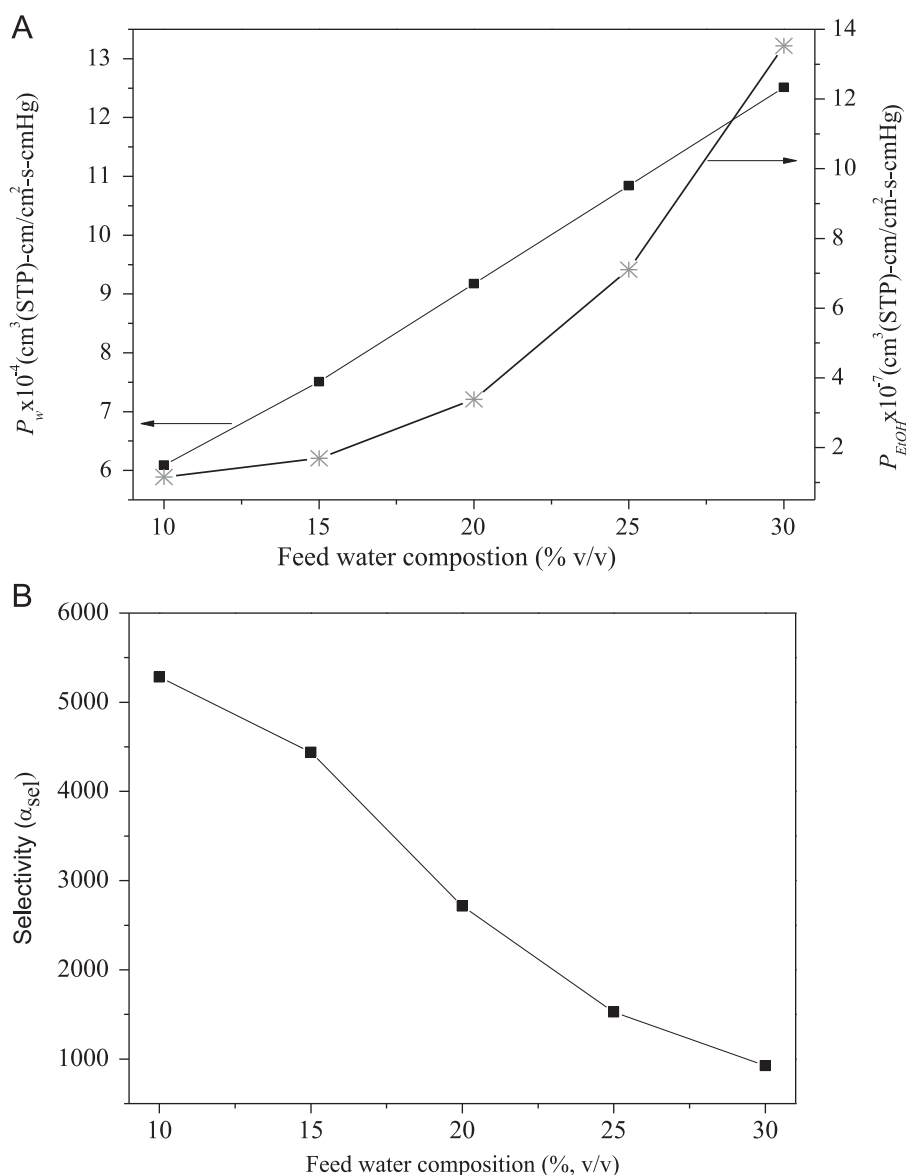


Fig. 13. Effect of feed water composition on (A)  $P_w$  and  $P_{EtOH}$ ; (B) selectivity factor: in PV performances of CPS-a membrane (thickness: 100  $\mu$ m) at 30 °C.

**Table 2**  
Comparative study PV performance of the present membrane with reported membrane.

Types of membrane	Membrane thickness ( $\mu$ m)	Temperature (°C)	Ethanol/alcohol in feed (wt%)	$J_{total}$ (kg/m <sup>2</sup> h)	$\alpha_{sel}$	Ref.
CSCM-30	32	70	90	0.41	1102	[19]
NCM-5	40	30	90	0.11	2725	[22]
PCS-3-3	150	30	90	0.44	3860	[24]
1	1	75	90	8	1000	[34]
CPS-a	100	30	90	0.59	5282	This study

pervaporation dehydration of ethanol–water mixture exhibited 0.11 kg/m<sup>2</sup> h flux and 2725  $\alpha_{sel}$  value at 30 °C, while CPS-a membrane reported in this work showed 0.59 kg/m<sup>2</sup> h flux and 5282  $\alpha_{sel}$  under similar experimental conditions [21]. Thus modification in the chitosan leads to an improvement in membrane permeability and selectivity factor for dehydration of the ethanol, compared to starting material. In particular,  $\alpha_{sel}$  value of CPS-a

membrane is much higher than those of others, and permeation flux is reasonable. Thus the PV performance is acceptable for the dehydration of ethanol especially for CPS-a membrane.

#### 4. Conclusions

Functionalized silica (SBAPTS)–NSBC hybrid membranes were prepared by sol–gel followed by cross-linking for PV separation of water/ethanol azeotrope. Degree of cross-linking depended on reaction conditions (formaldehyde concentration, cross-linking time and temperature). Cross-linking density for different membranes was also determined by DMA analysis, and showed 1.6 GPa storage modulus for highly cross-linked membrane, and indicated that membrane stiffness associated with decrease in free volume.

Prepared hybrid membrane, especially CPS-a, was assessed to be very suitable for the separation of water from azeotrope of water–ethanol with 5282 selectivity and 0.59 l m<sup>-2</sup> h total flux at 30 °C in ethanol/water mixture (90 wt%). Performances of these membranes were compared with reported membranes in the

literature, which suggested a potential use of prepared hybrid membrane (CPS-a) due to high flux and selectivity at low temperatures. Furthermore, chitosan provides a low-caste material and, utilization of functionalized chitosan–silica hybrid is novel and challenging, as it is inexpensive, nonhazardous, and environmentally benign.

## Acknowledgements

Ravi P. Pandey is thankful to the UGC for award of JRF. Instrumental support received from Analytical Science Division, CSMCRI, is also gratefully acknowledged.

## Appendix A. Supporting information

Supplementary data associated with this article can be found in the online version at <http://dx.doi.org/10.1016/j.memsci.2013.04.065>.

Nomenclature	
PV	Pervaporation
NSBS	<i>N</i> -o-sulphonic acid benzyl chitosan
SBAPTS	Sodium 2-formylbenzenesulfonatepolysiloxane
PVA	Poly(vinyl alcohol)
APTES	(3-Aminopropyl)triethoxysilane
THF	Tetrahydrofuran
TGA	Thermogravimetric analysis
DSC	Differential scanning calorimetry
DMA	Dynamic mechanical analyzer
TEM	Transmission electron microscope
AFM	Atomic force microscopy
SEM	Scanning electron microscopy
<i>S</i> (%)	Swelling ratio
<i>W</i> <sub>s</sub>	Weight swollen membrane
<i>W</i> <sub>d</sub>	Weight dry membrane
<i>J</i>	Flux
<i>Q</i>	Quantity of permeate (Kg)
<i>A</i>	Effective membrane area
IR	Infrared
<i>R</i> <sub>q</sub>	Surface roughness
EDX	Energy-dispersive X-ray spectroscopy
<i>T</i> <sub>g</sub>	Glass transition temperature
<i>ρ</i>	Cross-linking density of membrane
<i>d</i>	Membrane density
<i>φ</i>	Front factor
<i>R</i>	Universal gas constant
<i>T</i>	Absolute temperature
<i>E'</i>	Storage modulus
<i>P</i> <sub>w</sub>	Permeability of water
<i>P</i> <sub>EtOH</sub>	Permeability of ethanol
<i>α</i> <sub>sel</sub>	Selectivity data
<i>M</i> <sub>NaOH</sub>	molarity of NaOH
<i>x</i> <sub>i</sub>	Mole fraction of component <i>i</i>
<i>y</i> <sub>i</sub>	Mole fraction of component <i>i</i>
<i>γ</i> <sub>i</sub>	Activity coefficient
<i>P</i> <sub>i</sub> <sup>sat</sup>	Saturated vapour pressure of component <i>i</i>
<i>P</i> <sub>permeate</sub>	Vapour pressure in permeate side
<i>p</i> <sub>e</sub>	Partial pressure of ethanol
<i>p</i> <sub>w</sub>	Partial pressure of water

## References

- [1] P. Guo, C.R. Martin, Y. Zhao, J. Ge, R.N. Zare, General method for producing organic nanoparticles using nanoporous membranes, *Nano Lett.* 10 (2010) 2202–2206.
- [2] S.K. Choudhari, A.A. Kittur, S.S. Kulkarni, M.Y. Kariduraganavar, Development of novel blocked diisocyanate crosslinked chitosan membranes for pervaporation separation of water-isopropanol mixtures, *J. Memb. Sci.* 302 (2007) 197–206.
- [3] A. Kulkarni, K. De Frees, S.H. Hyun, D.H. Thompson, Pendant polymer: amino-β-cyclodextrin: siRNAGuest: host nanoparticles as efficient vectors for gene silencing, *J. Am. Chem. Soc.* 134 (2012) 7596–7599.
- [4] B. Thierry, F.M. Winnik, Y. Merhi, M. Tabrizian, Nanocoatings onto arteries via layer-by-layer deposition: toward the *in vivo* repair of damaged blood vessels, *J. Am. Chem. Soc.* 125 (2003) 7494–7495.
- [5] S. Prakash, T. Chakrabarty, A.K. Singh, V.K. Shahi, Silver nanoparticles built-in chitosan modified glassy carbon electrode for anodic stripping analysis of As (III) and its removal from water, *Electrochim. Acta* 72 (2012) 157–164.
- [6] B.P. Tripathi, V.K. Shahi, Functionalized organic–inorganic nanostructured N-p-carboxy benzyl chitosan–silica–PVA hybrid polyelectrolyte complex as proton exchange membrane for DMFC applications, *J. Phys. Chem. B* 112 (2008) 15678–15690.
- [7] Z. Zhao, J. Zheng, M. Wang, H. Zhang, C.C. Han, High performance ultrafiltration membrane based on modified chitosan coating and electrospun nanofibrous PVDF scaffolds, *J. Memb. Sci.* 394–395 (2012) 209–217.
- [8] K. Zielinska, W. Kujawski, A.G. Chostenko, Chitosan hydrogel membranes for pervaporative dehydration of alcohols, *Sep. Purif. Technol.* 83 (2011) 114–120.
- [9] Y.L. Liu, Y.H. Su, J.Y. Lai, In situ crosslinking of chitosan and formation of chitosan–silica hybrid membranes with using γ-glycidoxypropyltrimethoxysilane as a crosslinking agent, *Polymer* 45 (2004) 6831–6837.
- [10] R.Y.M. Huang, R. Pal, G.Y. Moon, Crosslinked chitosan composite membrane for the pervaporation dehydration of alcohol mixtures and enhancement of structural stability of chitosan/polysulfone composite membranes, *J. Memb. Sci.* 160 (1999) 17–30.
- [11] C.E. Schmidt, J.M. Baier, Acellular vascular tissues: natural biomaterials for tissue repair and tissue engineering, *Biomaterials* 21 (2000) 2215–2231.
- [12] S. Xiao, X. Feng, R.Y.M. Huang, Trimesoyl chloride crosslinked chitosan membranes for CO<sub>2</sub>/N<sub>2</sub> separation and pervaporation dehydration of isopropanol, *J. Memb. Sci.* 306 (2007) 36–46.
- [13] X.H. Zhang, Q.L. Liu, Y. Xiong, A.M. Zhu, Y. Chen, Q.G. Zhang, Pervaporation dehydration of ethyl acetate/ethanol/water azeotrope using chitosan/poly(vinyl pyrrolidone) blend membranes, *J. Memb. Sci.* 327 (2009) 274–280.
- [14] K. Sunitha, S.V. Satyanarayana, S. Sridhar, Phosphorylated chitosan membranes for the separation of ethanol–water mixtures by pervaporation, *Carbohydr. Polym.* 87 (2012) 1569–1574.
- [15] Y.T. Ong, A.L. Ahmad, S.H.S. Zein, K. Sudesh, S.H. Tan, Poly(3-hydroxybutyrate)-functionalised multi-walled carbon nanotubes/chitosan green nanocomposite membranes and their application in pervaporation, *Sep. Purif. Technol.* 76 (2011) 419–427.
- [16] Y. Liu, M. Zhu, Q. Zhao, Q. An, J. Qian, K. Lee, J. Lai, The chemical crosslinking of polyelectrolyte complex colloidal particles and the pervaporation performance of their membranes, *J. Memb. Sci.* 385–386 (2011) 132–140.
- [17] J. Ma, M. Zhang, H. Wu, X. Yin, J. Chen, Z. Jiang, Mussel-inspired fabrication of structurally stable chitosan/polyacrylonitrile composite membrane for pervaporation dehydration, *J. Memb. Sci.* 348 (2010) 150–159.
- [18] Y.L. Liu, C.Y. Hsu, Y.H. Su, J.Y. Lai, Chitosan–silica complex membranes from sulfonic acid functionalized silica nanoparticles for pervaporation dehydration of ethanol–water solutions, *Biomacromolecules* 6 (2005) 368–373.
- [19] Y.L. Liu, Y.H. Su, K.R. Lee, J.Y. Lai, Crosslinked organic–inorganic hybrid chitosan membranes for pervaporation dehydration of isopropanol–water mixtures with a long-term stability, *J. Memb. Sci.* 251 (2005) 233–238.
- [20] T. Uragami, S. Yamamoto, T. Miyata, Dehydration from alcohols by polyion complex cross-linked chitosan composite membranes during evaporation, *Biomacromolecules* 4 (2003) 137–144.
- [21] V.T. Magalad, G.S. Gokavi, M.N. Nadagouda, T.M. Aminabhavi, Pervaporation separation of water–ethanol mixtures using organic–inorganic nanocomposite Membranes, *J. Phys. Chem. C* 115 (2011) 14731–14744.
- [22] T. Uragami, T. Katayama, T. Miyata, H. Tamura, T. Shiraiwa, A. Higuchi, Dehydration of an ethanol/water azeotrope by novel organic–inorganic hybrid membranes based on quaternized chitosan and tetraethoxysilane, *Biomacromolecules* 5 (2004) 1567–1574.
- [23] B.P. Tripathi, M. Kumar, A. Saxena, V.K. Shahi, Bifunctionalized organic–inorganic charged nanocomposite membrane for pervaporation dehydration of ethanol, *J. Colloid Interface Sci.* 346 (2010) 54–60.
- [24] A. Betard, R.A. Fischer, Metal–organic framework thin films: from fundamentals to applications, *Chem. Rev.* 112 (2012) 1055–1083.
- [25] A.K. Singh, P. Singh, S. Mishra, V.K. Shahi, Anti-biofouling organic–inorganic hybrid membrane for water treatment, *J. Mater. Chem.* 22 (2012) 1834–1844.
- [26] R.K. Nagarale, J.M. Lee, W. Shin, Electrochemical properties of ferrocene modified polysiloxane/chitosan nanocomposite and its application to glucose sensor, *Electrochim. Acta* 54 (2009) 6508–6514.
- [27] A.N. Mondal, B.P. Tripathi, V.K. Shahi, Highly stable aprotic ionic-liquid doped anhydrous proton-conducting polymer electrolyte membrane for high-temperature applications, *J. Mater. Chem.* 21 (2011) 4117–4124.
- [28] B.P. Tripathi, V.K. Shahi, 3-[3-(Triethoxysilyl)propyl]amino]propane-1-sulfonic acid–poly(vinyl alcohol) cross-linked zwitterionic polymer electrolyte

- membranes for direct methanol fuel cell applications, *ACS Appl. Mater. Interfaces* 1 (2009) 1002–1012.
- [29] F. Peng, L. Lu, H. Sun, Y. Wang, J. Liu, Z. Jiang, Hybrid organic–inorganic membrane: solving the tradeoff between permeability and selectivity, *Chem. Mater.* 17 (2005) 6790–6796.
- [30] Z. Xie, E.J. Henderson, O. Dag, W. Wang, J.E. Lofgreen, C. Kubel, T. Scherer, P. M. Brodersen, Z.Z. Gu, G.A. Ozin, Periodic mesoporous hydridosilica—synthesis of an impossible material and its thermal transformation into brightly photoluminescent periodic mesoporous nanocrystal silicon–silica composite, *J. Am. Chem. Soc.* 133 (2011) 5094–5102.
- [31] M. Kumar, S. Singh, V.K. Shahi, Cross-linked poly(vinyl alcohol)–poly(acrylonitrile-co-2-dimethylamino ethylmethacrylate) based anion-exchange membranes in aqueous media, *J. Phys. Chem. B* 114 (2010) 198–206.
- [32] S. Singh, A. Jasti, M. Kumar, V.K. Shahi, A green method for the preparation of highly stable organic–inorganic hybrid anion-exchange membranes in aqueous media for electrochemical processes, *Polym. Chem.* 1 (2010) 1302–1312.
- [33] A.A. Kittur, M.Y. Kariduraganavar, U.S. Toti, K. Ramesh, T.M. Aminabhavi, Pervaporation separation of water-isopropanol mixtures using ZSM-5 zeolite incorporated poly(vinyl alcohol) membranes, *J. Appl. Polym. Sci.* 90 (2003) 2441–2448.
- [34] Q. Ge, Z. Wang, Y. Yan, High-performance zeolite NaA membranes on polymer zeolite composite hollow fiber supports, *J. Am. Chem. Soc.* 131 (2009) 17056–17057.